Inorganic Chemistry

Article

pubs.acs.org/IC

One-Pot Syntheses and Cell Imaging Applications of Poly(amino acid) Coated $LaVO_4:Eu^{3+}$ Luminescent Nanocrystals

Huanjie Wang and Leyu Wang*

State Key Laboratory of Chemical Resource Engineering, School of Science, Beijing University of Chemical Technology, Beijing 100029, People's Republic of China

Supporting Information

ABSTRACT: For successful biological applications of luminescent nanocrystals, surface functionalization is very essential. It is very important to develop the facile synthetic methods to gain access to obtaining water-stable and biocompatible NPs with appropriate functional groups as well as high luminescence efficiency. Herein, a green and facile one-pot hydrothermal strategy was developed for the preparation of poly(amino acid) coated $LaVO_4:Eu^{3+}$−PASP luminescent nanocrystals by employing the hydrolysis of polysuccinimide (PSI) to polyaspartic acid (PASP) to provide a general platform for the surface modification. Because of the enriched carboxylic groups in the PASP coating, these as-prepared nanoparticles (NPs) demonstrated good water-stability, biocompatibility, and bioconjugatability. Due to their strong red luminescence and good bioconjugatability, the antibody bioconjugated $LaVO_4:Eu^{3+}$−PASP NPs were successfully used as the biomarkers for cancer cell specific luminescence imaging. The results indicate that these NPs have the potential to act as luminescent probes for luminescence assay and in vitro imaging.

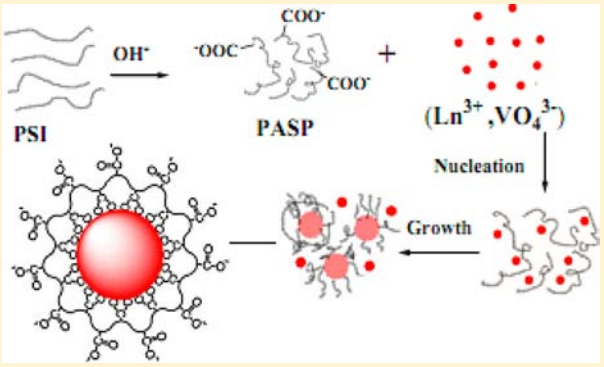

INTRODUCTION

Cell biology studies and biomedicine require powerful fluorescence imaging techniques of the single molecule scale to the whole studied organism, either for fundamental science or disease diagnosis.[1] Conventional biolabels including organic dyes[2] and quantum dots (QDs)[3−8] have already been employed in the fluorescence immunoassay, DNA detection, and in vivo/in vitro imaging. These applications are however often constrained by the chemical and optical stability of the fluorescence dyes and quantum dots (QDs).[9−11] As a kind of luminescent bioprobes, rare-earth-doped nanoparticles (NPs)[1,9,12−26]demonstrate great advantages such as wonderful chemical stability and photostability and have been widely used in the fields of luminescent detection,[11,23,24,27,28] in vivo/vitro imaging,[12,29] and so on.[11−13,30−37] However, for the biological applications, surface functionalization of the particles is a crucial step. The objective is first to ensure good dispersion of the particles in water. Second, particles should bare functional groups such as amino and carboxylic groups for bioconjugation.[22] A large pace of researches[30,38] into developing new luminescent materials, surface coatings, bioconjugation, and applications continues after the introduction of rare-earth luminescent materials to bioassays.

As a good matrix for red emission nanomaterials, lanthanum orthovanadate ($LaVO_4$) nanocrystals (NCs) have been widely investigated and many methods have been applied for the preparation of rare-earth-doped $LaVO_4$ NCs. $LaVO_4$ crystallizes in two polymorphs, namely, monoclinic (*m*-) monazite type and tetragonal (*t*-) zircon type.[39] *t*-$LaVO_4$ is expected to possess superior properties and is expected to be a promising phosphor candidate.[40,41] A general liquid−solid solution (LSS) method provided by Li's group[42−44] was used to prepare colloidal *t*-$LaVO_4:Eu^{3+}$ NCs assisted with oleic acid[34] molecules. Stouwdam et al.[31] selectively synthesized oil-soluble lanthanide-doped *m*- and *t*-$LaVO_4$ NPs by a precipitation reaction in the presence of $(C_{18}H_{37}O)_2PS_2$ as ligand. A few papers describe the selective-controlled structure and shape of $LaVO_4$ NCs without the presence of catalysts or templates via a hydrothermal treatment by tuning the pH of the growth solution.[39,45] It is noted that these NPs are hydrophobic or lack bioactive groups, most modification steps are complicated and time-consuming, and perhaps the chemical stability of modified NPs is reduced partly. Meanwhile, in most cases, the polymers used to functionalize the inorganic NPs, like poly(acrylic acid) (PAA)[13] and polyetherimide (PEI),[46] are unable to be biodegraded and sometimes cytotoxic. Therefore, the synthesis and application of biodegradable, biocompatible, and water-soluble polymers has become a hot spot in recent years. Polysuccinimide (PSI) is commonly used as the intermediate for the preparation of polyaspartic acid (PASP) and is able to hydrolyze in an alkaline environment, yielding water-soluble and biodegradable PASP.[47] Their chemical structures and the hydrolysis process are shown in Scheme 1.

Received: October 19, 2012
Published: February 18, 2013

   dx.doi.org/10.1021/ic302297u | *Inorg. Chem.* 2013, 52, 2439−2445

Scheme 1. Hydrolysis Process of Polysuccinimide in an Alkaline Environment

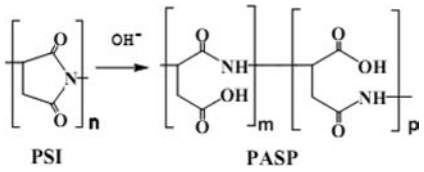

The lactam ring in the PSI chain is easily opened via aminolysis to form polyaspartic acid derivatives with a side-chain functional group. So far, PSI derivatives are mainly used to prepare hydrogels,[48] micelles,[49,50] or amphiphilic embedded polymers for encapsulation of NPs[51−53] and other applications.[54,55] PASP, the hydrolyzate of PSI under basic conditions, is a poly(amino acid) with a side-chain of carboxylic acid. Compared with aquogels of polymer including polyethylene glycol (PEG),[56] poly(acrylic acid) (PAA),[57] polyacrylamide (PAM),[58] polyvinyl pyrrolidone (PVP),[59] and so on, hydrogels of PASP have super hygroscopicity, biocompatibility, and negligible side effects and do not show antigenicity in the human body. So, it has become a new type of water-soluble and biodegradable functional material. At the same time, many drugs with $-NH_2$ groups can be linked to the chain of PASP via amide groups and form macromolecular drugs for controlled drug release.[50] But few documents in the literature report the one-pot fabrication of water-dispersible and biocompatible rare-earth-doped inorganic NPs coated with PASP derivatives for biomedical applications.

Recent improvements in colloid chemistry have allowed the investigation of other systems through the use of hydrothermal and solvothermal processes. This allows good control of nucleation/growth processes, leading to particles with an excellent crystallinity and a narrow size distribution.[1] Hence, we adopt the facile hydrothermal strategy for simultaneous synthesis and surface modification. In this work, a green, facile, and general one-pot hydrothermal strategy for the synthesis of *t*-$LaVO_4$:Eu^{3+}−PASP NPs with controlled particle size was successfully developed and these biocompatible NPs were used as biomarkers for cancer cell imaging. Scheme 2 showed the

Scheme 2. Schematic Illustration of the Growth Process for PASP-Coated $LaVO_4$:Eu^{3+} Nanoparticles

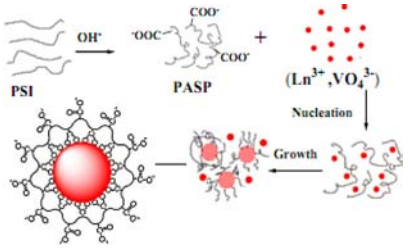

schematic illustration of the growth process of functional NPs. Please note that polysuccinimide (PSI), the original agent, is a polymer that can be hydrolyzed in alkaline aqueous solution, forming PASP with enriched carboxylic groups and other functional groups. PASP has great water-solubility and biodegradability. The poly(amino acid) solution might take part in the nucleation and growth process of rare-earth vanadate. They might have the chelating interaction between the carboxylate groups of PASP and rare-earth ions. Still, there are enough carboxylic groups on the particle surface, which helps to render the NPs water stable and bioconjugatable. Then, individual hydrophilic NPs were obtained and the as-synthesized luminescent NPs were successfully applied for targeted cell imaging.

EXPERIMENTAL SECTION

Chemicals and Reagents. $La(NO_3)_3{\cdot}6H_2O$ and $Eu(NO_3)_3{\cdot}6H_2O$ were purchased from Beijing Ouhe Chemical Reagents Company. Dimethyl sulfoxide (DMSO), paraformaldehyde, glycerin, NaOH, Na_2HPO_4, NaH_2PO_4, and NaCl were obtained from Beijing Chemical Reagent Company. Ammonium metavanadate (NH_4VO_3) was gained from Tianjin Fuchen Chemical Reagent Company. Polysuccinimide (PSI) (M_w = 6000) was kindly supplied by Shijiazhuang Desai Chemical Company. Methyl thiazolyl tetrazolium (MTT) was obtained from Sigma-Aldrich and used for the cytotoxicity test of the NPs. 1-Ethyl-3-(3-dimethyl-aminopropyl) carbodiimide (EDC, Sigma) and *N*-hydroxysuccinimide (NHS, Acros) were used as active agents for bioconjugation. Folic acid (FA) and alpha fetoprotein (AFP) was purchased from Beijing Aoboxing biotech and BaiTai biotech, respectively. Bovine serum albumin (BSA) was purchased from Sigma and used for surface blocking of the nanoparticles. Deionized (DI) water was used throughout the experiments. All reagents were analytical grade and used directly without further purification.

Characterization. The morphology and size of the as-prepared nanoparticles were obtained on a Hitachi H-800 transmission electron microscope (TEM) with a tungsten filament at an accelerating voltage of 200 kV. A scanning electron microscope (SEM, ZEISS Supra 55) was also used to observe the surface properties of samples. Fourier-transform infrared (FTIR) spectra were examined with a Nicolet 670 Fourier-transform infrared spectrophotometer by using KBr pellets. The optical properties of the NPs were conducted with a Hitachi F-4600 fluorescence spectrophotometer with a xenon discharge lamp as the excitation source. The decay time curve was recorded by an Edinburgh Instruments' FLS 920 instrument with a 450 W Xe arc lamp and a red sensitive Peltier element cooled Hamamatsu R955 PMT. An X-ray powder diffractometer (Rigku, D/max-Ultima III) with Cu Kα radiation (λ = 1.5402 Å) was used to record the X-ray diffraction (XRD) patterns of the sample. The operation voltage and current were controlled at 40 kV and 40 mA, respectively. The 2θ range used in the measurement was from 10° to 60° at a scanning rate of 10°/min. Zeta potential and dynamic light scattering (DLS) measurements were performed by using a Malvern Zetasizer 3000HS nanogranularity analyzer. Simultaneous thermal analyzer TGA/DSC 1/1100 SF (METTLER TOLEDO) was used for thermogravimetric analysis (TGA) with heating rate of 10 °C/min under N_2 atmosphere. Cell imaging experiment was conducted on a confocal laser scanning microscope (Leica TCS SP5) fitted with a wavelength at 700 nm as the two-photon laser excitation source. The transfection efficiency was analyzed on a BD FACSAria II Flow Cytometer with a fixed 375 nm laser.

Preparation of PASP-Functionalized $LaVO_4$:Eu^{3+} NPs. PASP-functionalized $LaVO_4$:Eu^{3+} nanoparticles were synthesized through a facile one-pot hydrothermal method. In a typical synthesis, NaOH (120 mg), PSI (0.1 g), and NH_4VO_3 (0.1 mmol) were dissolved into 35 mL of DI water under stirring. And then 1.0 mL of rare-earth solution (1.0 M, 98% La^{3+}, 2% Eu^{3+}) was slowly added to the mixture solution and the stirring was maintained for another 20 min. The obtained colloidal solution was transferred into a 50-mL Teflon-lined stainless steel autoclave and sealed. The autoclave was heated at 140 °C for 8 h and then cooled to room temperature naturally. The as-prepared nanoparticles were washed three times with DI water to remove any remaining reactants. The final product was redispersed in DI water and stored at room temperature for later use. As a control, the $LaVO_4$:Eu^{3+} nanoparticles without the PASP coating were also prepared in the absence of PASP via the same synthetic protocol for $LaVO_4$:Eu^{3+}−PASP.

dx.doi.org/10.1021/ic302297u | *Inorg. Chem.* 2013, 52, 2439−2445

Cytotoxicity Test of the NPs. In vitro cytotoxicity was measured by performing MTT assays[60] on the HeLa cell lines. Cells were seeded into a 96-well cell culture plate under 100% humidity and then cultured at 37 °C and 5% CO_2 for 24 h. $LaVO_4$:Eu^{3+}−PASP colloidal solution (100 μL per well) at final concentrations of 0, 10, 20, 30, 40, 50, 60, 80, 100, and 120 μg/mL were added into the wells, respectively, and further incubated for 24 or 48 h at 37 °C under 5% CO_2. Thereafter, MTT (20 μL, 5 mg/mL) dissolved in DMSO was added to each well and the plate was incubated for another 4 h. After the addition of DMSO (150 μL), the assay plate was agitated for 10 min. The absorbance of each well was measured at 490 nm by means of a Tecan Infinite (F50) microplate reader.

Bioconjugation of NPs with FA and AFP. The method for folic acid bioconjugation onto the $LaVO_4$ NPs was similar to the reported method.[61,62] Briefly, carboxylic acid enriched $LaVO_4$−PASP NPs (5.0 mg) were dispersed into 4.5 mL of phosphate buffer solution (PBS, Na_2HPO_4 8.0 mM, NaH_2PO_4 2.0 mM, NaCl 80 mM, pH 7.4), and then EDC (100 μL, 0.01 M) and NHS (100 μL, 0.01 M) were added into the vial and agitated for about 30 min to activate the carboxylic groups. Subsequently, 0.5 mL of DMSO containing FA (5 mg) was added to the above-mentioned solution of mixture under stirring at room temperature for 2 h. Excess FA, EDC, and NHS were removed by centrifugation, and the FA functionalized NPs (NPs-FA) were washed with PBS. The NPs were dispersed into 4.0 mL of PBS for later modification. Thereafter, 2.0 mg of BSA was added to the above solution, and the mixture was incubated for another 2 h at room temperature to block the spare carboxyl groups. The NPs-FA nanocomposites were purified with centrifugation and dispersed in PBS (4.0 mL). The stock solution was stored at 4 °C for use. The AFP antibody-labeled nanoparticles (NPs-AFP) were fabricated in the similar procedure as above.

Cell Imaging. For optical imaging, the HeLa and HepG2 cells growing in log phase were seeded onto the circular coverslips before being placed into a 6-well cell culture plate and cultured at 37 °C for 24 h. Thereafter, the cells were cultured with suitable concentration of NPs-FA (or NPs-AFP) nanocomposites for another 4 h. The cells were washed three times with 0.1 M PBS to remove the nanoparticles ungrafted onto the cells. These cells labeled with NPs were then fixed on the slip by using 4% paraformaldehyde and glycerin/PBS solution. And then, the slides were washed three times with PBS. Nanoparticles attached onto the fixed cells were then observed under a confocal laser scanning microscope (Leica TCS SP5) fitted with a wavelength of 700 nm as the two-photon laser excitation source.

Flow Cytometry Analysis.[63,64] Take the efficiency of NPs-FA to HeLa cell lines as an example. The sample preparation was similar to those used for cell imaging. The difference is that HeLa cells were seeded at the density of 10^6 cells per well in the 6-well tissue culture plate. After incubation with NPs-FA (30 μg/mL) at 37 °C for 4 h, HeLa cells were trypsinized, washed with PBS again, centrifuged, and resuspended in FACS buffer. FACS analysis was carried out on a BD FACSAria II Flow Cytometer with a fixed 375 nm laser. Data from 20 000 events/sample were gated using forward and side scatter parameters to exclude debris and dead cells. Cells without NP incubation were used as a negative control.

RESULTS AND DISCUSSION

The crystal size and morphology of the as-prepared NCs were studied by the transmission electron microscopy (TEM) and scanning electron microscopy (SEM). Figure 1a shows the TEM image of the typical $LaVO_4$:Eu^{3+}−PASP NPs. Viewed in-plane, the NCs are rectangle in shape with size of 34.8 ± 5.3 nm in length and width of 20.0 ± 2.6 nm, which are obtained by counting 200 nanoparticles from TEM micrograph. In addition, some larger sized particles are also observed in the image, which may be caused by the assembly of smaller rodlike nanoparticles.[42] Meanwhile, the SEM image of PASP-enriched $LaVO_4$ is also depicted in Figure 1b. These rodlike NPs are with width of 17.6 ± 2.8 nm and length of 38.3 ± 6.3 nm. This

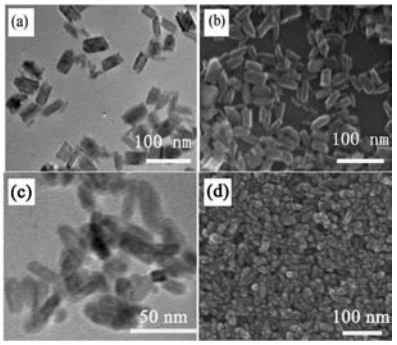

Figure 1. TEM (a and c) and SEM (b and d) images of the PASP-coated $LaVO_4$:Eu^{3+} nanoparticles (a and b) and uncoated $LaVO_4$:Eu^{3+} NPs (c and d).

result coincides with that shown in TEM images. It is notable that the shape of the $LaVO_4$:Eu^{3+} NPs without PASP coating is pretty irregular and the phenomenon of particle agglomeration is more serious (TEM and SEM images are shown in Figure 1c and d, respectively). The average diameter determined by DLS of $LaVO_4$:Eu^{3+}−PASP NPs was much smaller than that of those bare NPs without PASP coating (see Supporting Information Figure S1). These results indicated that the presence of PASP on the surface of NPs was in favor of the smaller size distribution.

Both the bare $LaVO_4$:Eu^{3+} without PASP coating and PASP-functionalized $LaVO_4$:Eu^{3+}−PASP NPs were also characterized by powder X-ray diffraction (XRD). The XRD patterns of $LaVO_4$:Eu^{3+} and $LaVO_4$:Eu^{3+}−PASP are provided in Figure 2.

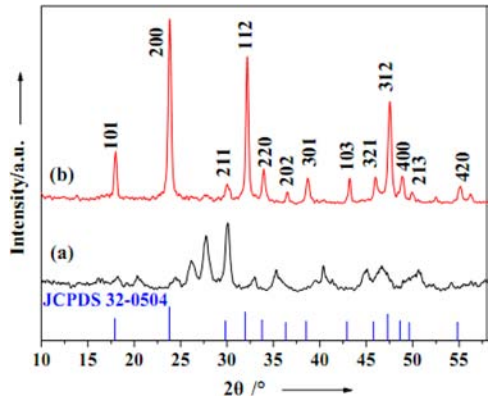

Figure 2. XRD patterns of $LaVO_4$:Eu^{3+} without PASP coating (a) and $LaVO_4$:Eu^{3+}−PASP (b) nanoparticles.

As shown in Figure 2a, bare $LaVO_4$:Eu^{3+} NPs prepared in water are mixed crystals with various phase composition. Most XRD peaks could be the combination of monazite phase of $LaVO_4$ (JCPDS no. 50-0367) and zircon-type $LaVO_4$ (JCPDS no. 32-0504). As depicted in the pattern of $LaVO_4$:Eu^{3+}−PASP (Figure 2b), the sharp peaks at 17.9°, 23.8°, 33.8°, and 48.6° are very remarkable. They are indexed to the ⟨101⟩, ⟨200⟩, ⟨220⟩, and ⟨400⟩ reflections of zircon-type $LaVO_4$ (space group: $I4_1/amd$) with lattice constants $a = b = 7.49$ Å and $c = 6.433$ Å (JCPDS card 32-0504).[42] The intensity of other peaks is not very strong. But the position and relative intensities of all diffraction peaks matches well with the t-$LaVO_4$:Eu^{3+} (JCPDS card 32-0504). No peaks of any other phases or impurities are examined. This can be attributed to the strong chelating interaction between the carboxylate groups of PASP and rare-

dx.doi.org/10.1021/ic302297u | Inorg. Chem. 2013, 52, 2439−2445

earth ions, which results in slow nucleation and good crystallization. The XRD results of the nanocrystals indicate that the presence of PASP contributes to higher crystallinity and phase purity. From the XRD patterns, the crystallite sizes are calculated using Debye−Scherrer's relation, $d = 0.89\lambda/(\beta \cos \theta)$, where d is average grain size and λ is the X-ray wavelength, while θ and β are the diffraction angle and full width at half-maximum. The crystallite sizes obtained by the Scherrer's equation from the width of the (200) and (103) peaks in the XRD patterns are c.a. 22 and 41 nm, respectively, which correspond well with the width and length of the rodlike nanoparticles, respectively, measured from the TEM and SEM images.

The surface properties of the as-prepared $LaVO_4:Eu^{3+}$−PASP nanocrystals were characterized by FTIR spectroscopy shown in Figure 3. In the FTIR pattern of PSI shown in Figure 3a, the

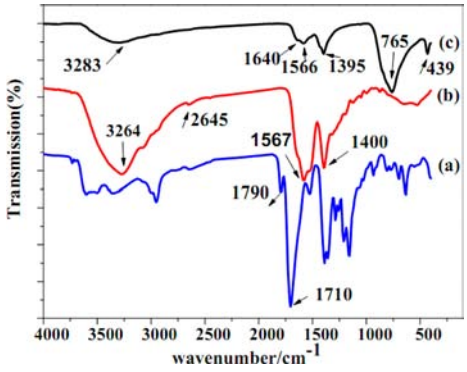

Figure 3. FTIR spectra of PSI (a), PASP (b), and $LaVO_4:Eu^{3+}$−PASP NPs (c).

absorption peak at 1710 and 1790 cm^{-1} were assigned as the vibration of the intra-annular imide, which was caused by the coupling reaction of adjacent carboxyl groups of the intra-annular imide in the chain of PSI.[50,65] If more NaOH was added, more PSI was hydrolyzed to PASP. Just as shown in Figure 3b, the characteristic absorption bands of intra-annular imide at 1710 and 1790 cm^{-1} disappeared. This illustrated that PSI was ring-opened and more amide groups and −COOH groups were formed in the chain (Scheme 1). The broad band at 3264 cm^{-1} and small peak at 2645 cm^{-1} were characteristic of the O−H (COO−H) stretching vibration. The bands at 1567 and 1400 cm^{-1} were assigned to asymmetric (υ_{as}) and symmetric (υ_s) stretching vibrations of the carboxylate group, respectively.[12] Most peaks in the FTIR spectrum of the $LaVO_4:Eu^{3+}$−PASP (NPs-PASP) (Figure 3c) were similar to those of PASP (Figure 3b). The absorption around 3283 cm^{-1} was assigned to O−H (COO−H) stretching vibration arising from PASP or water absorption. The absorptions around 1640 and 1566 cm^{-1} were the characteristic absorption of amide bands. The peak at 1395 cm^{-1} was due to the C−O symmetric stretching vibration (υ_s) in the −COOH groups of PASP. The band at 1566 cm^{-1} also could be identified as asymmetric (υ_{as}) stretching vibration of the carboxylate group.[66] In general, the intensity of the asymmetric C−O band of dissociative carboxyl groups should be stronger than that of the symmetric one. The $-COO^-$ groups in different chemicals coordinate to rare-earth ions in different ways, which may lead to some changes in the intensity of stretching vibration in the −COOH groups.[67,68] The broad peak observed around 765 cm^{-1} was attributed to the V−O vibration. The sharp band at 439 cm^{-1} was assigned to the VO_4^{3-} vibration.[41,66] These results were powerful evidence for the existence of the PASP on the surface of the $LaVO_4:Eu^{3+}$ NPs.

The surface charge of the materials was also characterized via zeta potential measurements at various pH values (Figure S2 in the Supporting Information). The initial zeta potential value of PASP-modified $LaVO_4:Eu^{3+}$ NPs has been measured to be −40.0 mV in DI water, which is much more negative than that of bare NPs (−1.40 mV) without PASP coating. The zeta potentials of NPs with PASP modification were near neutral at pH 2.5 and became negative with increasing pH, consistent with the weak acidity of −COOH groups.[69,70] The results indicate that the PASP has been successfully coated onto the surface of $LaVO_4:Eu^{3+}$ NPs, which is in favor of the narrow size distribution and good water stability.

The surface coating of as-prepared NPs were further investigated by TGA analysis with heating rate of 10 °C/min under N_2 atmosphere. Figure 4 illustrated the multistep TG

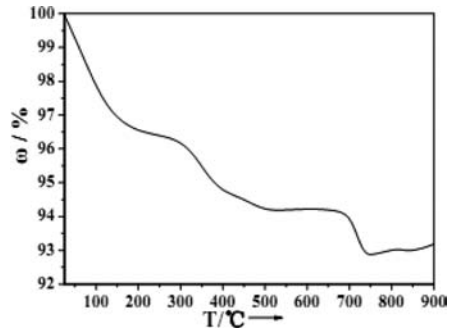

Figure 4. TGA curve of $LaVO_4:Eu^{3+}$−PASP NPs.

curves for $LaVO_4:Eu^{3+}$-PASP NPs. The first slow weight loss at around 50−160 °C could be explained by the evaporation of absorbed water molecules .The second weight loss at 270−550 °C and the third weight loss around 700 °C might be attributed to the thermal decomposition of different molecular weight PASP on the outermost surface of NPs. During the preparation of PASP-functionalized $LaVO_4:Eu^{3+}$ NPs, the presence of NaOH would lead to the partial hydrolysis of PSI to PASP. But the excessive NaOH in the reaction system would further make the hydrolyzation of long-chain PSI under high temperature conditions. That is why two different decomposition stages appeared. The remaining weight of the NPs was 93%. This result further inferred that PASP was coated onto the surface of $LaVO_4:Eu^{3+}$ NPs, which was in accordance with the FTIR results shown in Figure 3.

Figure 5a and 5b show the excitation and emission spectra of $LaVO_4:Eu^{3+}$-PASP colloids, respectively. The main excitation peak is ranging from 250 to 350 nm. The strong peak around 310 nm results from the light scattering that is about half of the main emission at 620 nm.[32] The emission spectrum of $LaVO_4:Eu^{3+}$−PASP aqueous solution shown in Figure 5b includes a weak emission band at 595 nm and a strong emission peak at 620 nm. They can be assigned to the transitions of $^5D_0-^7F_1$ (λ = 595 nm) and $^5D_0-^7F_2$ (λ = 620 nm) of Eu^{3+} ions, respectively.[66] The dominant red emission is centered at 620 nm with the excitation at 254 nm. Figure 5c also gives the optical photos of the $LaVO_4:Eu^{3+}$−PASP aqueous colloid solution. It is obvious that the transparent NPs solution have excellent water-solubility. Furthermore, the sample solution can be preserved steadily for more than 6 months. Under the UV

dx.doi.org/10.1021/ic302297u | Inorg. Chem. 2013, 52, 2439−2445

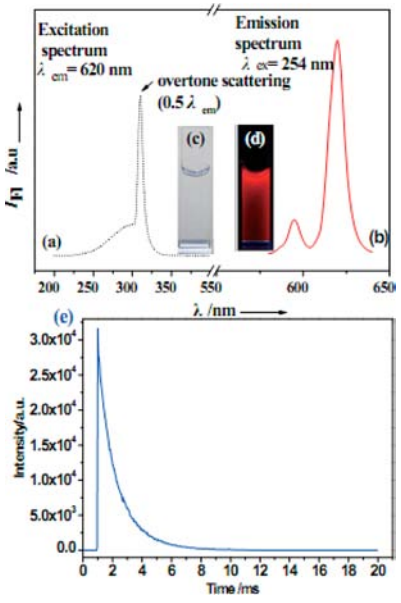

Figure 5. Excitation (a) and emission (b) spectra of $LaVO_4$:Eu^{3+}−PASP NPs, optical photos of the NPs under daylight (c) and UV lamp (d) with excitation at 254 nm and (e) luminescence decay curves (λ_{ex} = 254 nm, λ_{em} = 620 nm) of sample.

excitation of 254 nm, the sample can emit bright red luminescence (Figure 5d). The naked-eye visible luminescence emission fully explains the as-prepared rare-earth-doped nanomaterials have good luminescence emission characteristics. Figure 5e showed the luminescence decay curves of Eu^{3+} in $LaVO_4$:Eu^{3+}−PASP NPs .The decay curves can be well-fitted into a biexponential decay function as $I = I_0 + B_1 \exp(-t/\tau_1) + B_2 \exp(-t/\tau_2)$, where τ_1 and τ_2 were the decay time. The lifetimes of 1834 μs (τ_1, 59.54%) and 949 μs (τ_2, 40.46%) were obtained, respectively. The average decay time was calculated to be 1476 μs. The result almost corresponds to some reported literature.[31,71] The strong luminescence intensity and good water stability of NPs lays a good foundation for the applications of biological luminescence quantification and in vitro imaging.

To demonstrate the potential use of $LaVO_4$:Eu^{3+}−PASP NPs in bioimaging applications, we tested the cytotoxicity of $LaVO_4$:Eu^{3+}−PASP NPs toward HeLa cell lines by MTT assay. Upon incubation with 0−120 μg/mL of $LaVO_4$:Eu^{3+}−PASP, the cellular viabilities were examined with the MTT assays. As shown in Figure 6, when the concentration of NPs

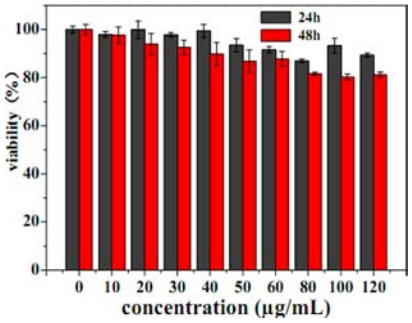

Figure 6. Cell viability estimated by MTT assay in HeLa cell lines which were cultured in the presence of 0−120 μg/mL $LaVO_4$:Eu^{3+}−PASP NPs at 37 °C for 24 and 48 h, respectively.

reached 120 μg/mL, the viability was estimated to be greater than 86% and 80% after incubation for 24 and 48 h, respectively. If only 20 μg/mL of NPs was added, about 99% and 97% of the cells were alive after 24 and 48 h, respectively. After incubation with 40 μg/mL of NPs for 24 h, the cellular viability was greater than 99%, and the cell viability still remained over 92% when the incubation time was prolonged to 48 h. These data of MTT assays attest that the $LaVO_4$:Eu^{3+}−PASP NPs have considerable low cytotoxicity. It should be mentioned that these NPs are highly luminescent and a pretty low concentration is enough for the cell imaging application. According to the strong red luminescence and the results of the cytotoxicity tests, 30 μg/mL as the final concentration was adopted for use in the following luminescence imaging experiments.

The strong red luminescence and good water-dispersibility implied that the NPs have the potential to be good biolabels in luminescence imaging. In general, most biological tissues often emit green background luminescence under UV excitation. But our rare-earth-doped materials emit unique red light, the biological autofluorescence can be greatly overcome if the $LaVO_4$:Eu^{3+}−PASP NPs are applied for luminescence imaging as biomarkers. Furthermore, the presence of free carboxylic acid groups on the surface of PASP-capped NPs facilitates further bioconjugation with various biomolecules.

In view of the highly specific interaction between alpha fetoprotein (AFP) antibody and AFP on the surface of hepatocarcinoma cells, when the cells were incubated with NPs-AFP nanocomposites, they could be recognized by HepG2 cells. Upon the two-photon laser excitation with a wavelength at 700 nm, the HepG2 cells exhibited bright red luminescence of NPs (Figure 7a). The shape and position of the cells in bright field and luminescence mode overlaps very well, suggesting that the red luminescence is from the NPs attached onto the cell surface. These results demonstrated the good specific interaction between the NPs-AFP and HepG2 cells. To the best of our knowledge, both HeLa and HepG2 cancer cells are overexpressed with folic acid (FA) receptors on the cell membrane. When they were incubated with NPs-FA nanocomposites, they could be labeled by the red luminescence of the attached NPs. As shown in Figure 7c, the FA coated NPs were attached onto the HepG2 cells.

To further testify the specific recognition ability of the functionalized NPs for targeted luminescence imaging, the two kinds of bioconjugated NPs (NPs-FA, NPs-AFP) were incubated with HeLa cells and the luminescence was checked with two-photon imaging. The HeLa cells were incubated with NPs-AFP in the same physiological conditions as a negative control to verify the specific recognition and combination between the NPs-AFP and the HepG2 cells. Because NPs-AFP cannot be recognized specifically by the HeLa cells, no red luminescence was observed on the cell surface (Figure 7b). Due to the existence of folic acid (FA) antigens overexpressed by the HeLa cells, the NPs-FA particles were specifically attached onto the HeLa cells and emitted red luminescence (Figure 7d). The results indicated that the NPs with good biocompatibility recognized the targets on the cell membrane due to the AFP conjugation, and the luminescence intensity was strong enough for cell imaging applications. Furthermore, flow cytometry is usually considered as a powerful protocol for cell imaging efficiency evaluation. Take the efficiency of NPs-FA labeling HeLa cell lines as an example, a graphical representation of the dot plot data illustrated the percentage of cell conjugated with

dx.doi.org/10.1021/ic302297u | Inorg. Chem. 2013, 52, 2439−2445

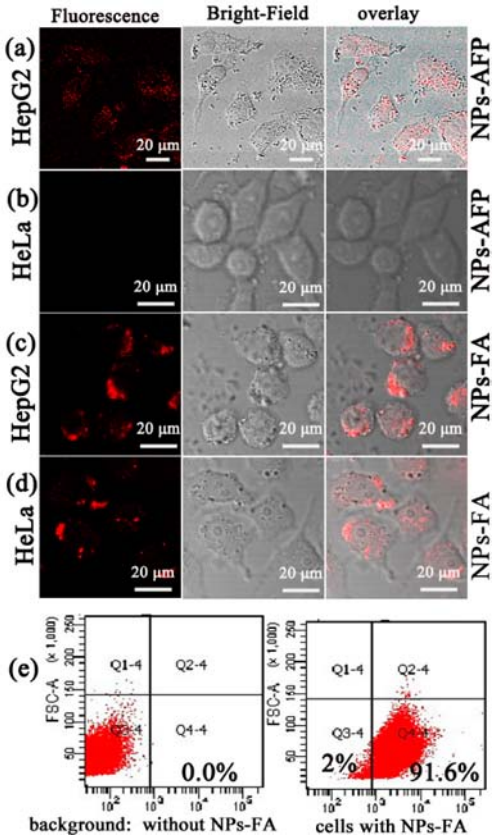

Figure 7. Two-photon luminescence images of HepG2 and HeLa cells after incubation with 30 μg/mL of NPs-AFP (a and b) and NPs-FA (c and d) for 4 h at 37 °C (λ_{ex} = 700 nm) and flow cytometry analysis (e) of HeLa cells before (left) and after (right) transfection with NPs-FA for 4h.

NPs-FA was shown in Figure 7e. Compared with cells without NPs-FA treatment, HeLa cells yield 91.6% transfection efficiency for $LaVO_4$. The results showed that high efficient transfection was taking place in the majority of analyzed HeLa cell cultures. This further proved the credibility of our cell-imaging results.

CONCLUSION

In summary, we have successfully developed a green and facile one-pot strategy to fabricate $LaVO_4$:Eu^{3+}−PASP nanoparticles with strong red emission. Due to the biocompatible PASP coating layer, these as-prepared colloidal NPs are highly water-stable, biocompatible, and bioconjugatable. After being conjugated with specific bioprobes such as AFP antibodies, the NPs can be specifically recognized by the target cancer cells for targeted luminescence imaging. We anticipate that the water-stable NPs will have promising applications for luminescence immunoassays and cell imaging. In addition, this method should also be capable of extension to the direct synthesis of other water-stable and bioconjugatable inorganic nanomaterials.

ASSOCIATED CONTENT

Supporting Information

Figures S1 and S2. This material is available free of charge via the Internet at http://pubs.acs.org.

AUTHOR INFORMATION

Corresponding Author

*E-mail: lywang@mail.buct.edu.cn.

Notes

The authors declare no competing financial interest.

ACKNOWLEDGMENTS

This work was supported in part by the National Natural Science Foundation of China (Grant Nos. 21075009, 21275015), the State Key Project of Fundamental Research of China (2011CB932403, 2011CBA00503), and the Program for New Century Excellent Talents in University of China (NCET-10-0213).

REFERENCES

(1) Bouzigues, C.; Gacoin, T.; Alexandrou, A. *ACS Nano* **2011**, *5*, 8488−8505.
(2) Zhang, M.; Yu, M. X.; Li, F. Y.; Zhu, M. W.; Li, M. Y.; Gao, Y. H.; Li, L.; Liu, Z. Q.; Zhang, J. P.; Zhang, D. Q.; Yi, T.; Huang, C. H. *J. Am. Chem. Soc.* **2007**, *129*, 10322−10323.
(3) Liu, H. Y.; Gao, X. H. *Bioconjugate Chem.* **2011**, *22*, 510−517.
(4) Zrazhevskiy, P.; Sena, M.; Gao, X. H. *Chem. Soc. Rev.* **2010**, *39*, 4326−4354.
(5) Hu, X. G.; Gao, X. H. *ACS Nano* **2010**, *4*, 6080−6086.
(6) Bruchez, M., Jr.; Moronne, M.; Gin, P.; Weiss, S.; Alivisatos, A. P. *Science* **1998**, *281*, 2013−2016.
(7) Chan, W. C.; Nie, S. *Science* **1998**, *281*, 2016−2018.
(8) Gao, X. H.; Cui, Y. Y.; Levenson, R. M.; Chung, L. W. K.; Nie, S. M. *Nat. Biotechnol.* **2004**, *22*, 969−976.
(9) Chen, Z. G.; Chen, H. L.; Hu, H.; Yu, M. X.; Li, F. Y.; Zhang, Q.; Zhou, Z. G.; Yi, T.; Huang, C. H. *J. Am. Chem. Soc.* **2008**, *130*, 3023−3029.
(10) Wang, L. Y.; Li, Y. D. *Nano Lett.* **2006**, *6*, 1645−1649.
(11) Wang, L. Y.; Yan, R. X.; Hao, Z. Y.; Wang, L.; Zeng, J. H.; Bao, H.; Wang, X.; Peng, Q.; Li, Y. D. *Angew. Chem., Int. Ed.* **2005**, *44*, 6054−6057.
(12) Deng, M. L.; Ma, Y. X.; Huang, S.; Hu, G. F.; Wang, L. Y. *Nano Res.* **2011**, *4*, 685−694.
(13) Wang, L. Y.; Zhang, Y.; Zhu, Y. Y. *Nano Res.* **2010**, *3*, 317−325.
(14) Heer, S.; Lehmann, O.; Haase, M.; Güdel, H. U. *Angew. Chem., Int. Ed.* **2003**, *42*, 3179−3182.
(15) Bunzli, J. C. G. *Chem. Rev.* **2010**, *110*, 2729−2755.
(16) Zhou, J.; Liu, Z.; Li, F. *Chem. Soc. Rev.* **2012**, *41*, 1323−1349.
(17) Grzyb, T.; Lis, S. *Inorg. Chem.* **2011**, *50*, 8112−8120.
(18) Huang, C. H.; Chen, T. M.; Cheng, B.-M. *Inorg. Chem.* **2011**, *50*, 6552−6556.
(19) Li, G.; Peng, C.; Zhang, C.; Xu, Z.; Shang, M.; Yang, D.; Kang, X.; Wang, W.; Li, C.; Cheng, Z.; Lin, J. *Inorg. Chem.* **2010**, *49*, 10522−10535.
(20) Li, X.; Gai, S.; Li, C.; Wang, D.; Niu, N.; He, F.; Yang, P. *Inorg. Chem.* **2012**, *51*, 3963−3971.
(21) Qu, X.; Yang, H. K.; Pan, G.; Chung, J. W.; Moon, B. K.; Choi, B. C.; Jeong, J. H. *Inorg. Chem.* **2011**, *50*, 3387−3393.
(22) An, M. Y.; Cui, J. B.; He, Q.; Wang, L. Y. *J. Mater. Chem. B.* **2013**, *1*, 1333−1339.
(23) Ma, Y. X.; Li, H.; Peng, S.; Wang, L. Y. *Anal. Chem.* **2012**, *84*, 8415−8421.
(24) Ma, Y. X.; Li, H.; Wang, L. Y. *J. Mater. Chem.* **2012**, *22*, 18761−18767.
(25) Wang, L. Y.; Li, P.; Li, Y. D. *Adv. Mater.* **2007**, *19*, 3304−3307.
(26) Wang, L. Y.; Li, Y. D. *Chem. Mater.* **2007**, *19*, 727−734.
(27) Li, H.; Wang, L. Y. *Analyst.* **2013**, *138*, 1589−1595.
(28) Li, H.; Wang, H. J.; Wang, L. Y. *J. Mater. Chem. C.* **2013**, *1*, 1105−1110.
(29) Deng, M. L.; Tu, N. N.; Bai, F.; Wang, L. Y. *Chem. Mater.* **2012**, *24*, 2592−2597.

(30) Ansari, A. A.; Alam, M.; Labis, J. P.; Alrokayan, S. A.; Shafi, G.; Hasan, T. N.; Syed, N. A.; Alshatwi, A. A. *J. Mater. Chem.* **2011**, *21*, 19310−19316.
(31) Stouwdam, J. W.; Raudsepp, M.; van Veggel, F. *Langmuir* **2005**, *21*, 7003−7008.
(32) Wang, L.; Li, P.; Wang, L. Y. *Luminescence* **2009**, *24*, 39−44.
(33) Pichaandi, J.; Boyer, J. C.; Delaney, K. R.; van Veggel, F. *J. Phys. Chem. C* **2011**, *115*, 19054−19064.
(34) Johnson, N. J. J.; Oakden, W.; Stanisz, G. J.; Prosser, R. S.; van Veggel, F. *Chem. Mater.* **2011**, *23*, 3714−3722.
(35) Boyer, J. C.; Manseau, M. P.; Murray, J. I.; van Veggel, F. *Langmuir* **2010**, *26*, 1157−1164.
(36) Wang, J.; Wang, F.; Wang, C.; Liu, Z.; Liu, X. G. *Angew. Chem., Int. Ed.* **2011**, *50*, 10369−10372.
(37) Wang, F.; Deng, R. R.; Wang, J.; Wang, Q. X.; Han, Y.; Zhu, H. M.; Chen, X. Y.; Liu, X. G. *Nat. Mater.* **2011**, *10*, 968−973.
(38) Xu, Z. H.; Li, C. X.; Hou, Z. Y.; Peng, C. O.; Lin, J. *Crystengcomm* **2011**, *13*, 474−482.
(39) Fan, W. L.; Song, X. Y.; Bu, Y. X.; Sun, S. X.; Zhao, X. *J. Phys. Chem. B* **2006**, *110*, 23247−23254.
(40) Jia, C. J.; Sun, L. D.; Luo, F.; Jiang, X. C.; Wei, L. H.; Yan, C. H. *Appl. Phys. Lett.* **2004**, *84*, 5305−5307.
(41) Jia, C. J.; Sun, L. D.; You, L. P.; Jiang, X. C.; Luo, F.; Pang, Y. C.; Yan, C. H. *J. Phys. Chem. B* **2005**, *109*, 3284−3290.
(42) Liu, J. F.; Li, Y. D. *Adv. Mater.* **2007**, *19*, 1118−1122.
(43) Liu, J. F.; Li, Y. D. *J. Mater. Chem.* **2007**, *17*, 1797−1803.
(44) Wang, X.; Zhuang, J.; Peng, Q.; Li, Y. D. *Nature* **2005**, *437*, 121−124.
(45) Fan, W. L.; Bu, Y. X.; Song, X. Y.; Sun, S. X.; Zhao, X. A. *Cryst. Growth Des.* **2007**, *7*, 2361−2366.
(46) Kievit, F. M.; Veiseh, O.; Bhattarai, N.; Fang, C.; Gunn, J. W.; Lee, D.; Ellenbogen, R. G.; Olson, J. M.; Zhang, M. Q. *Adv. Funct. Mater.* **2009**, *19*, 2244−2251.
(47) Lee, H. J.; Yang, S. R.; An, E. J.; Kim, J. D. *Macromolecules* **2006**, *39*, 4938−4940.
(48) Spadaro, G.; Dispenza, C.; Giammona, G.; Pitarresi, G.; Cavallaro, G. *Biomaterials* **1996**, *17*, 953−958.
(49) Arimura, H.; Ohya, Y.; Ouchi, T. *Biomacromolecules* **2005**, *6*, 720−725.
(50) Lin, W.; Kim, D. *Langmuir* **2011**, *27*, 12090−12097.
(51) Jana, N. R.; Erathodiyil, N.; Jiang, J.; Ying, J. Y. *Langmuir* **2010**, *26*, 6503−6507.
(52) Koga, H.; Toita, R.; Mori, T.; Tomiyama, T.; Kang, J. H.; Niidome, T.; Katayama, Y. *Bioconjugate Chem.* **2011**, *22*, 1526−1534.
(53) Zhang, Z. P.; Gao, D. M.; Zhao, H.; Xie, C. G.; Guan, G. J.; Wang, D. P.; Yu, S. H. *J. Phys. Chem. B* **2006**, *110*, 8613−8618.
(54) Lee, H. Y.; Jee, H. W.; Seo, S. M.; Kwak, B. K.; Khang, G.; Cho, S. H. *Bioconjugate Chem.* **2006**, *17*, 700−706.
(55) Uchida, H.; Miyata, K.; Oba, M.; Ishii, T.; Suma, T.; Itaka, K.; Nishiyama, N.; Kataoka, K. *J. Am. Chem. Soc.* **2011**, *133*, 15524−15532.
(56) Koh, W. G.; Itle, L. J.; Pishko, M. V. *Anal. Chem.* **2003**, *75*, 5783−5789.
(57) Jang, S. S.; Goddard, W. A.; Kalani, M. Y. S. *J. Phys. Chem. B* **2007**, *111*, 1729−1737.
(58) Dinu, M. V.; Perju, M. M.; Dragan, E. S. *Macromol. Chem. Phys.* **2011**, *212*, 240−251.
(59) Jiao, Y. P.; Liu, Z. H.; Ding, S.; Li, L. H.; Zhou, C. R. *J. Appl. Polym. Sci.* **2006**, *101*, 1515−1521.
(60) Duan, H. W.; Nie, S. M. *J. Am. Chem. Soc.* **2007**, *129*, 3333−3338.
(61) Bharali, D. J.; Lucey, D. W.; Jayakumar, H.; Pudavar, H. E.; Prasad, P. N. *J. Am. Chem. Soc.* **2005**, *127*, 11364−11371.
(62) Yang, S. J.; Lin, F. H.; Tsai, K. C.; Wei, M. F.; Tsai, H. M.; Wong, J. M.; Shieh, M. J. *Bioconjugate Chem.* **2010**, *21*, 679−689.
(63) Abbasi, M.; Uludag, H.; Incani, V.; Hsu, C. Y. M.; Jeffery, A. *Biomacromolecules* **2008**, *9*, 1618−1630.
(64) Yang, Z.; Sahay, G.; Sriadibhatla, S.; Kabanov, A. V. *Bioconjugate Chem.* **2008**, *19*, 1987−1994.
(65) Seo, K.; Kim, D. *Macromol. Biosci.* **2006**, *6*, 758−766.
(66) Okram, R.; Singh, N. R.; Singh, A. M. *Micro. Nano Lett.* **2011**, *6*, 165−169.
(67) Yu, H.; He, Q. Z.; Yang, J.; Zheng, W. J. *J. Rare Earths* **2006**, *24*, 4−8.
(68) Zolin, V. F.; Puntus, L. N.; Tsaryuk, V. I.; Kudryashova, V. A.; Legendziewicz, J.; Gawryszewska, P.; Szostak, R. *J. Alloy. Compd.* **2004**, *380*, 279−284.
(69) Gentili, P. L.; Presciutti, F.; Evangelisti, F.; Costantino, F. *Chem.—Eur. J.* **2012**, *18*, 4296−4307.
(70) Shyue, J. J.; De Guire, M. R.; Nakanishi, T.; Masuda, Y.; Koumoto, K.; Sukenik, C. N. *Langmuir* **2004**, *20*, 8693−8698.
(71) Zhao, M. L.; Li, G. S.; Zheng, J.; Li, L. P.; Wang, H.; Yang, L. S. *Crystengcomm* **2011**, *13*, 6251−6257.